The Space Congress® Proceedings

1976 (13th) Technology For The New Horizon

Apr 1st, 8:00 AM

Photoelectrolysis Of Water By Solar Energy

D. I. Tchernev

Lincoln Laboratory, Massachusetts Institute of Technology, Lexington, Massachusetts 02173

PHOTOELECTROLYSIS OF WATER BY SOLAR ENERGY*

D. I. Tchernev
Lincoln Laboratory, Massachusetts Institute of Technology
Lexington, Massachusetts 02173

ABSTRACT

The direct conversion of solar energy to chemical fuel is possible by photodecomposition of water on semiconducting electrodes. We have observed 100% quantum efficiency for this reaction without corrosion of the electrodes. Projected costs of large area, thin film devices, utilizing existing technology, indicate that the hydrogen fuel can be cost competitive with other fuels now.

INTRODUCTION

Although the free energy required for the decomposition of water into gaseous H_2 and O_2 is only 1.23 eV, while the peak of the solar spectrum occurs at a photon energy of about 2.4 eV, solar energy cannot be utilized for the production of H_2 fuel by the direct photodecomposition of water, because the threshold energy for this direct reaction is about 6.5 eV. Fujishima and Honda have recently shown, however, that this threshold can be greatly reduced if decomposition is accomplished by means of photoelectrolysis, a process in which a semiconductor is used as a catalyst. These authors immersed Pt and single-crystal TiO_2 electrodes in an aqueous electrolyte and connected them externally to form an electrolytic cell. When the semiconducting n-type TiO_2 was illuminated, current flowed in the external circuit, and the liberation of O_2 and H_2, respectively, occurred at the TiO_2 and Pt electrodes, provided that the photon energy exceeded 3.0 eV, the energy gap of TiO_2. Unlike many other n-type semiconductors, the TiO_2 did not undergo anodic dissolution.

On the basis of the results reported by Fujishima and Honda, photoelectrolysis is a promising process for the large-scale utilization of solar energy to produce H_2 fuel. In order to further evaluate its potential for this application, we have been investigating the physics and electrochemistry of photoelectrolysis by experiments on cells with polycrystalline as well as single-crystal TiO_2 anodes. This work then led to studies with $SrTiO_3$ anodes and we report some of these results as well.

ENERGY DIAGRAM OF A PHOTOELECTROLYSIS CELL

Figure 1 is an energy diagram of a basic photoelectrolysis cell consisting of an n-type semiconducting working electrode, an electrolyte, and a Pt counterelectrode. Because of the difference in work functions between the semiconductor and the electrolyte, the energy bands of the semiconductor are bent at the surface, so that the analog of a Schottky barrier exists at the semiconductor-electrolyte interface. The semiconductor surface is irradiated by photons of energy at least equal to its energy gap. The photon-generated hole-electron pairs do not recombine but are separated by the electric field of the barrier; the electrons move away from the surface into the bulk of the semiconductor and then through the external circuit to the Pt cathode, where they discharge $H_2(2e^- + 2H^+ \rightarrow H_2)$, while the holes remain at the surface of the semiconductor anode, where they can interact with the electrolyte to produce $O_2(2p^+ + H_2O \rightarrow 1/2\ O_2 + 2H^+)$. The overall chemical reaction is

$$2h\nu + H_2O \rightarrow 1/2\ O_2 + H_2 \qquad (1)$$

provided the semiconductor is chemically inert, serving only to absorb the light and to produce the holes and electrons that make the reaction possible. Two conditions are necessary for efficient photoelectrolysis: (1) The energy bands at the semiconductor-electrolyte interface must be bent in order to separate the holes and electrons excited by the light and (2) the relevant electronic levels must line up, i.e., the hole states of the anode with $\mathcal{E}(H_2O/O_2)$ and the Fermi level of the cathode with $\mathcal{E}(H^+/H_2)$.

EXPERIMENTS WITH TiO_2 ANODES

The anode material used in most of our experiments was the rutile form of TiO_2. Some TiO_2 anodes were fabricated from single crystals, but most were polycrystalline disks prepared by hot-pressing powdered rutile at 750°C under a pressure of 10,000 psi. To make the disks conducting ($\rho \sim 10^3\ \Omega$-cm), they were heated in vacuum for three hours at ~ 600°C, which causes a loss of oxygen that makes them n-type and gives them a blue coloration. Other anodes were prepared by heating Ti foils at ~ 600°C in an oxygen atmosphere for periods of three hours or more to form polycrystalline TiO_2 films by thermal oxidation.

In initial experiments we measured the band bending in TiO_2 as a function of electrolyte pH by using both the differential space charge capacitance and surface photovoltage techniques to determine the flat-band potential. This is the potential of the semiconductor electrode (with respect to a reference electrode -- in our case the saturated calomel electrode) at which the bands are not bent. With increasing pH, the flat-band potential (and thus the band bending) was found to vary linearly with a slope of 0.059 eV/pH (i.e., 2.303 e/kT), as expected if the principal effect of the change in pH is to vary the Fermi level in the solution.

*This work was sponsored by the Defense Advanced Research Projects Agency and the Department of the Air Force.

The operating characteristics of electrochemical photocells under constant illumination from a 150-W Xe source were measured for various values of pH. Typical results, obtained for pH = 0, are plotted in Figure 2. The upper curve gives the output voltage, V, as a function of the current drawn from the cell per cm^2 of illuminated TiO_2 surface. The lower curve gives the electrical power, P, extracted by the load. For maximum gas production, the cell is operated in the short circuit mode; for this example, the current density $J_{SC} = 1.88$ mA/cm^2. If the cell is operated at $J < J_{SC}$, electrical power can be extracted at the same time as gas is discharged. The two curves in Figure 2 can be fit to a fairly good approximation by a model that considers the electrochemical photocell as a constant voltage source in series with an internal resistance. Here, the open circuit voltage is 0.52 V and the internal resistance is $\sim 350\ \Omega$.

In order to check whether the rate-limiting step was the generation of electron-hole pairs, we investigated the dependence of J_{SC} on light intensity (with photons at $h\nu \sim 4$ eV, which as discussed below is the energy of peak response of the cell). The dependence is linear at low intensity, but begins to saturate at intensities higher than about 5 mW/cm^2. On a clear day, the intensity of solar radiation within the 3 to 4 eV spectral region is between 2 and 4 mW/cm^2 in the linear-response region.

The external quantum efficiency, η, as a function of photon energy, $h\nu$, was measured on an optimized electrochemical photocell for light intensities in the linear region. The anode was illuminated by monochromatic light from a source consisting of a 1000-W Xe lamp and a grating monochromator. The light intensity, S, incident on the cell was measured as a function of $h\nu$ by means of a thermopile power meter that had a flat response down to 0.25 μm. The value of η, defined as the ratio of the number of electrons flowing in the external circuit (N_e) to the number of photons incident on the cell (N_p), was calculated at each value of $h\nu$ from

$$\eta \equiv \frac{N_e}{N_p} = \frac{\dfrac{J_{sc}(A/cm)^2}{e\ (Coul)}}{\dfrac{S(W/cm^2)}{h\nu(eV) \times e\ (Coul)}} = \frac{J_{sc}}{S} h\nu \ . \qquad (2)$$

Figure 3 shows the values of η vs $h\nu$ for a single crystal and for a hot-pressed disk (both measured in a buffered electrolyte with pH = 8). The maximum values of η, 82% for the single crystal and 60% for the polycrystalline disk, occur at $h\nu \approx 4$ eV.

Quantum efficiency measurements were also made with TiO_2 films on Ti foil that had been thermally oxidized. The results for two such films, prepared under different conditions and measured in a non-buffered electrolyte of pH 13, are shown in Figure 4. For film "a" (7 μm thick), η reaches a maximum value of 84% at $\lambda = 3400$ Å (~ 3.5 eV), while film "b" (< 2 μm thick) has a maximum of 83% at 3000 Å (~ 4 eV). The positions of the quantum efficiency peaks in Figures 3 and 4 correspond to 3 major absorption peaks in TiO_2 that occur at about 3.5, 4 and 4.7 eV (3400, 3000 and 2600 Å) respectively. The relative intensities of the efficiency peaks depend on preparation procedure and oxide layer thickness.

When the maximum measured η values are corrected by taking account of estimated reflection losses at the interfaces and absorption losses in the electrolyte, we find that the internal quantum efficiency is close to 100% for both single-crystal and polycrystalline TiO_2 anodes. This high quantum efficiency shows that the band bending in TiO_2 is sufficient to separate the electron-hole pairs generated by photon absorption and in addition that the hole states of the anodes line up with the (H_2O/O_2) level of the electrolyte. As stated above, however, for efficient photoelectrolysis it is also necessary for the Fermi level of the cathode, $\mathcal{E}_F$, to line up with the electrochemical potential of the H^+/H_2 level in the solution, $\mathcal{E}(H^+/H_2)$.

The quantum efficiency experiments just described were performed with the photoelectrolysis cell open to air, so that the electrolyte contained dissolved oxygen. In this case, it is seen from Figure 1 that the energetically favorable process at the cathode is the transfer of electrons from the cathode (at $\mathcal{E}_F$) to the H_2O/O_2 level, causing the reduction of oxygen:

$$\frac{1}{2} O_2 + H_2O + 2e^- \rightarrow 2\,OH^- \ . \qquad (3)$$

The cell now functions in the galvanic mode, and no H_2 gas is evolved. Under these conditions, we have observed that the O_2 bubbles formed at the anode migrate to the cathode, where they disappear.

This obstacle to the production of H_2 gas can be eliminated by removing the dissolved oxygen from the cathode compartment of the cell, either by bubbling an inert gas such as N_2 or Ar through the solution or by pumping on the solution with a vacuum pump. However, the cell current then decreases considerably, so that η becomes only 1-2%, even for the best TiO_2 anodes. This decrease occurs because of the energy difference associated with electron transfer from $\mathcal{E}_F$ to the higher-lying (H^+/H_2) level. This energy difference, which varies from sample to sample of TiO_2, has a minimum value of 0.2 eV. There is a small amount of current flow because the energy states of the solution are broad enough to partially overlap $\mathcal{E}_F$.

There are several possible methods for obtaining a better match between $\mathcal{E}_F$ and $\mathcal{E}(H^+/H_2)$ in order to increase the efficiency of H_2 production. One method is simply to apply a small external voltage of about 1/4 V. Another is to use an H-shaped cell with a strongly basic solution in the anode compartment and a strongly acidic solution in the cathode compartment, separated from each other by a low-resistance ion exchange membrane. This method utilizes the electromotive force due to the difference in solution pH, $\mathcal{E} \approx 0.059\Delta[\mathrm{pH}]$, to obtain level matching. A quantum efficiency of $\sim 10\%$ has been reported for hydrogen generation using this procedure. Although the heat of neutralization is ~ 15.9 kcal/mole, there is a considerable net gain in energy, because the heat of combustion of hydrogen is 68 kcal/mole. However the method is inconvenient because the solutions are gradually neutralized as the cell operates, and the energy matching deteriorates.

EXPERIMENTS WITH $SrTiO_3$ Anodes

The $SrTiO_3$ anodes used in the experiments reported here were n-type disks 5 to 15 mm in diameter that had

been cut from a single crystal (Titanium Pigment Division of National Lead Industries). Preliminary experiments with an anode prepared by pressing powdered $SrTiO_3$ gave results similar to those obtained with single-crystal material. The material was reduced by annealing in H_2 at atmospheric pressure for about 3 hours at 900°C. After reduction $SrTiO_3$ changed from insulating to conducting, with a resistivity ~ 15 Ω-cm, and from colorless and transparent to blue-black and opaque. An ohmic contact was made to each disk by ultrasonically soldering In to its back surface and attaching a Pt wire to the In. The entire disk, except for the front surface, was then coated with insulating epoxy or stop-off lacquer.

Again photoelectrolytic cells were prepared by immersing a $SrTiO_3$ anode and a platinized-Pt cathode into an aqueous electrolyte contained in a fused-quartz vessel. Each electrode was capped with an inverted buret filled with electrolyte, so that the gas evolved could be collected by liquid displacement for volumetric measurement and chemical analysis. Provision was made for flushing the electrolyte with either N_2 or Ar in order to remove dissolved O_2 so that the cell operated in the photoelectrolytic mode. Measurements were generally made after the solution had been purged for several hours.

Figure 5 is a plot of the variation of AC photocurrent with electrode potential at pH = 13.3. One can use such a plot to estimate the flat band potential from the value of voltage at which the photocurrent goes to zero. Two curves are shown here --one for TiO_2 and the other from $SrTiO_3$. Also shown is the equilibrium hydrogen potential $\mathcal{E}(H_2/H^+)$ for this pH. These results indicate that the band bending for photoelectrolysis is very small for TiO_2 and ~ 0.2 volts more for $SrTiO_3$. This is consistent with the difference in work function, or electron affinity, of ~ 0.2 volt as measured by the Kelvin contact potential method in air.

This ~ 0.2 volt increase in band bending results in a quantum efficiency for photoelectrolysis of 10% at $h\nu = 3.8$ eV. This is about one order of magnitude larger than that found for TiO_2. The gases evolved at the electrodes were collected and analyzed. At high pH values (pH > 13) the volumes of gas collected at the cathode and anode were found to be over 90% of the values calculated from the integrated electrocurrent by assuming that only the reaction given by Eq. (1) is taking place. These results are consistent with the conclusion that photoelectrolysis is the only reaction occurring.

Finally, the proposed arrangement whose band diagram is shown in Figure 6 is potentially the most successful. Here, both electrodes are working electrodes, with a p-type semiconductor replacing the platinum cathode. The cell is spatially arranged so that the incident radiation arrives first at the anode, with energy gap $E_g(n)$, and then at the cathode, with a lower gap $E_g(p)$. The anode absorbs the photons with energies higher than $E_g(n)$ and transmits those with lower energies to the cathode. Thus a large portion of the solar spectrum can be utilized. Bending of the energy bands is necessary at both electrode-electrolyte interfaces. The bands of the p-type semiconductor should be bent downward to trap electrons for the cathode reaction responsible for H_2 discharge. With a band bending of ~ 0.3 eV at each interface, for electrolysis the sum of the two energy gaps must be

$$E_g(n) + E_g(p) \geq 1.23 + b_n + b_p \geq 1.8 \text{ eV} \quad ,$$

where b_n and b_p are the amounts of band bending at the anode and cathode, respectively. This arrangement requires the Fermi level of the p-type electrode to lie below the electrochemical potential of the electrolyte by several tenths of an eV, and the Fermi level of the n-type electrode to lie a similar energy above it. Moreover, at the surface of the p-type semiconductor the bottom of the conduction band must fall at or above the H^+/H_2 level in the electrolyte, which is about 4.5 eV below the vacuum level. This arrangement has not yet been optimized because a completely suitable p-type semiconductor has not yet been identified.

Whatever method is employed to obtain the required matching of energy levels between the cathode and the electrolyte, the efficiency with which solar energy can be utilized to generate H_2 by photoelectrolysis will ultimately depend on the semiconductors that are used as electrode materials. Only about 10% of the solar energy reaching the earth is supplied by photons with energies higher than 3.0 eV, the energy gap of TiO_2 or $SrTiO_3$. Therefore the efficiency of solar utilization will be limited to a few percent unless it is possible to find a suitable electrode material with a significantly lower energy gap.

CHEMICAL STABILITY

The stability of semiconductors under illumination in an electrolyte is determined mainly by the position of the valence band of the semiconductor relative to the energy of the redox reaction in the solution. For n-type semiconductors in the depletion mode, the optically created holes arrive at the electrode-electrolyte interface because of the electric field existing in the depletion layer. At this interface there are two possible competing reactions: 1) the oxidation of ions from the solution, yielding an electron that recombines with the hole in the semiconductor; 2) the dissolution of the semiconductor, with the ions that go into solution transferring their electrons to the semiconductor. The second reaction is the more favorable one in most well-known semiconductors like Si, GaAs, CdS, etc.

From simple energy considerations it is clear that if the valence band of the semiconductor lies higher than the energy of the redox reaction, no oxidation will be possible since the electrons must move up in energy. In this case the hole arriving at the surface represents a broken bond in the valence band. The surface atoms of the semiconductor already have bonds with fewer neighbors than the bulk atoms; therefore such a broken bond (hole) reduces the binding energy of the surface atoms even further. If thermal lattice vibrations are not sufficient to break the atom loose, a second hole arriving at the same atom will complete the dissolution.

The main stability criteria for a n-type semiconductor under illumination is therefore a deep valence band. For example, TiO_2 has an electron affinity of about 4 eV; i.e., its conduction band lies at about 4 eV below the vacuum level. Since its energy gap is 3 eV, its

valence band is about 7 eV below the vacuum level. Since the normal hydrogen electrode reaction is at 4.5 eV below the vacuum level, the oxygen evolution reaction is at 5.75 eV below vacuum or about 1.25 eV above the valence band of TiO_2. The presence of small negative surface charge (in this case occupied surface states) lowers the bands of the semiconductor by another 0.2 to 0.3 eV with respect to the liquid. The oxidation of OH^- radicals on TiO_2 then occurs via surface states (believed to be due to Ti^{3+} ions) which are roughly centered in the middle of the energy gap. These states and their position in energy have been identified independently by two different methods and the agreement is excellent.

Finally a few words about economics. Using spray techniques it is possible to deposit thin films of TiO_2 on glass with SnO_2 transparent contacts for about $\$3/m^2$. Including the cost of $\$5/m^2$ for container, counter-electrode and deployment, the total cost of a photoelectrolysis cell in mass production can be about $\$8/m^2$. If the semiconductor is only 10% efficient at decomposing water utilizing the light in the solar spectrum above 3 eV, for a system lifetime of 20 years the cost of producing gaseous hydrogen fuel will be about $\$5.30/10^6$ BTU, which is competitive with the present cost of heating oil of between \$8 and $\$9/10^6$ BTU.

With a semiconductor of a smaller band gap, for example, 1.7 eV and 30% quantum efficiency, the cost of hydrogen would drop to $\$1/10^6$ BTU even if it were necessary to use deposited thin films at an additional cost of $\$13.50/m^2$. This would make hydrogen cost competitive even with natural gas, which is presently regulated at an artificially low price. This indicates that the photoelectrolysis of water is a very promising method for utilizing solar energy to produce chemical fuel in an efficient and inexpensive way.

ACKNOWLEDGEMENT

The information presented in this paper resulted from the cooperative efforts of a team consisting of the author, John Mavroides, James Kafalas, and Donald Kolesar.

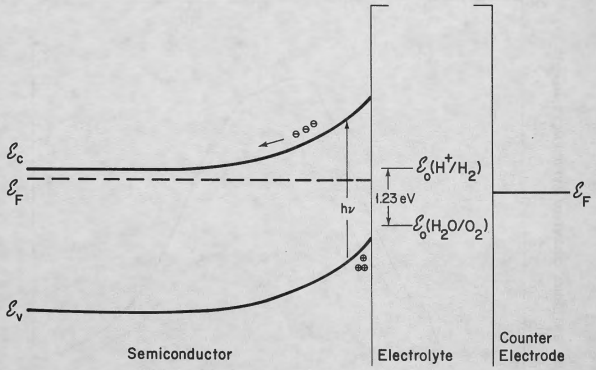

Figure 1. Energy diagram of the semiconductor-electrolyte boundary.

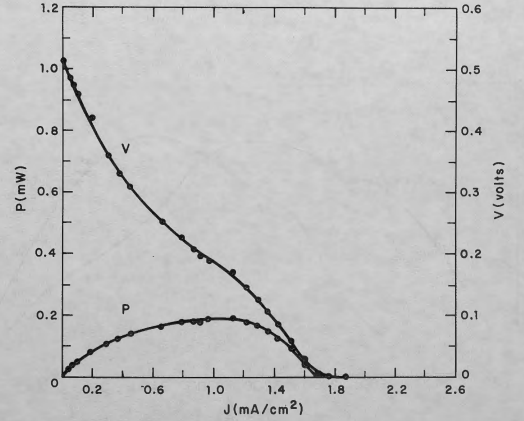

Figure 2. Current-voltage and power characteristics of a TiO_2 electrochemical photocell.

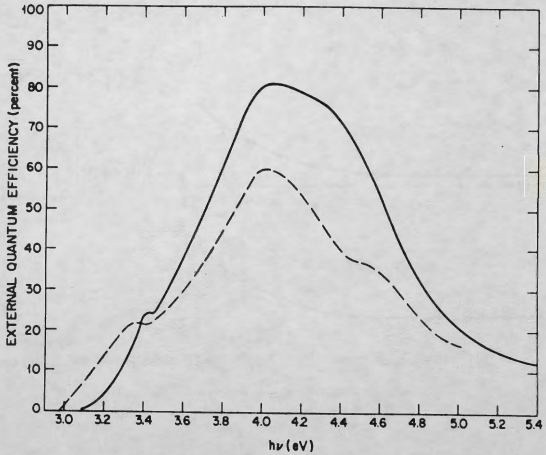

Figure 3. Quantum efficiency as a function of frequency for a single crystal and hop-pressed TiO_2 sample.

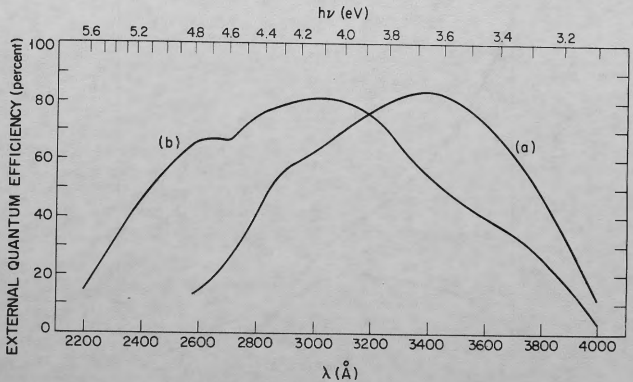

Figure 4. Quantum efficiency curves for thermally oxidized titanium foils.

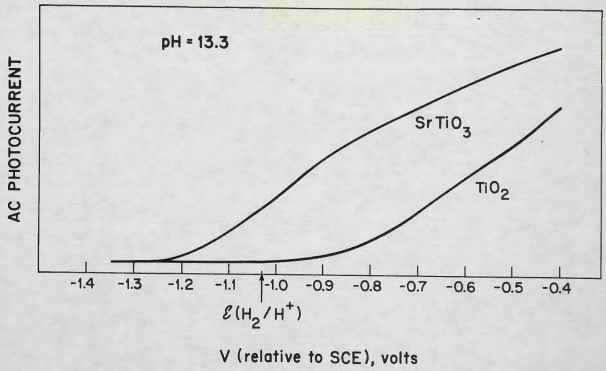

Figure 5. Photocurrent-potential plot for TiO_2 and $SrTiO_3$.

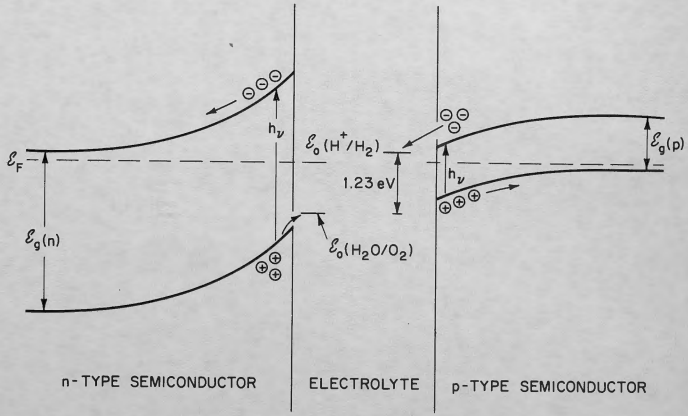

Figure 6. Energy band diagram for the proposed p-n double electrode cell.

USE OF SATELLITES TO DETERMINE OPTIMUM LOCATIONS FOR SOLAR POWER STATIONS

Dr. H. W. Hiser and Prof. H. V. Senn
Remote Sensing Laboratory
School of Engineering and Environmental Design
University of Miami
Coral Gables, Florida 33124

ABSTRACT

Ground measurements of solar radiation are too sparse to determine important mesoscale differences that can be of major significance in solar power station locations. Cloud images in the visual spectrum from the SMS/GOES geostationary satellites are used to determine the hourly distribution of sunshine on a mesoscale in the continental United States excluding Alaska. Cloud coverage and density as a function of time of day and season are considered through the use of digital data processing techniques. Low density cirrus clouds are less detrimental to solar energy collection than other types; and clouds in the morning and evening are less detrimental than those during midday hours of maximum insolation.

The seasonal geographic distributions of sunshine are converted to Langleys of solar radiation received at the earth's surface through the use of transform equations developed from long-term measurements of these two parameters at 18 widely distributed stations. The high correlation between measurements of sunshine and radiation makes this possible. The output product will be maps showing the geographic distribution of total solar radiation on the mesoscale which is received at the earth's surface during each season.

INTRODUCTION

Intermediate scale (mesoscale) differences in the distribution of solar radiation received at the earth's surface can be very important in selecting the location for a large solar energy station. Daily totals and in some cases hourly records of solar insolation exist for about 54 National Weather Service and 27 Cooperative stations in the 48 contiguous United States [1]. Generalized maps have been drawn by use of data from these stations, but they cannot depict the mesoscale differences. There are some excellent prospective power sites within areas that are mostly nominal quality, and there are some poor sites within areas that are generally high quality.

Since clouds of the "low-cloud family," including those of vertical development, tend to be thick and contain lots of moisture, they are the major absorbers or attenuators of incoming solar radiation. These low cloud types are most responsive to surface features such as localized heating or cooling, coastal effects, and topography. This responsiveness is manifest in the time, space, and density distributions of these low cloud types. These localized differences in the low-cloud family are the major cause of mesoscale differences in solar radiation reaching the earth.

There are two types of solar radiation measurements commonly made at the earth's surface, direct and total. Direct is that received directly from the sun and is measured on a flat surface normal to the sun's rays. The Eppley normal incidence pyrheliometer is a typical instrument used for this. Total radiation is the direct plus that reflected from all parts of the sky, and it is measured on a horizontal flat surface. The Eppley model II pyranometer is a typical instrument for this measurement. At many stations, daily totalizers are used on both types of instruments. At some stations, analog chart recorders are used so that the time distribution and hourly totals of radiation can be obtained [1]. Eighteen of the National Weather Service pyranometer stations that have analog chart recorders, which provide hourly radiation data, also have sunshine switches with recorders that provide minutes of sunshine per hour. The sunshine switches are calibrated to indicate sunshine so long as enough sunlight is present for nearby objects to cast a shadow. Thus periods with high thin clouds are recorded as sunshine. Depending upon the threshold of the switch, heavier clouds may also register as sunshine.

In this study, total solar radiation received per hour is correlated with minutes of sunshine per hour recorded at 18 surface stations in different climatic and air quality regions of the United States. The SMS/GOES geostationary satellites provide mesoscale images of cloud cover and conversely sunshine by hours of the day. The ground station relations between sunshine and total radiation are used to transform the satellite measurements of sunshine into equivalent solar radiation data. Computer processing of the data provides seasonal mapping of sunshine and solar radiation on the mesoscale [2]. Early research on the use of satellites to measure solar energy was conducted by Fritz, et al. [3]. More recent works relating to the subject include Thekaekara [4], Hanson [5], and Vonder Haar [6].

In addition to cloudiness, latitude, season of the year, time of day, and air quality (turbidity, etc.) are important factors in solar insolation. Cloudiness with respect to time of day is important because morning and evening cloudiness is less detrimental than that at midday. This can be particularly important if a high temperature solar concentrator is to be used, in which case, the midday high energy hours of sunshine would be most valuable. The geostationary satellite observations throughout the day provide these hourly distributions of cloudiness and sunshine.

Our ground station data used to write the transforms from sunshine to solar radiation are from 18 stations throughout the United States. For example, Great Falls, Montana, data will be applied to the northern high plains and data for Boston, Mass., will be used to develop transform relations for the northeastern seaboard. This system will automatically compensate for differences in air quality in our results because each station will be fairly representative of its region.

DATA SOURCES

Daytime satellite imagery from the Stationary Meteorological Satellite (SMS-1) is being used to provide cloud data for 1975. The bulk of the data will be from the visual channel (.55-.75μ) of SMS-1 located at 75°W longitude over the equator; but in order to adequately cover the western portions of the country later in the afternoon, it will be necessary to either use output from SMS-2 (at 115°W longitude for most of the year) or from the infrared channels of SMS-1. Since SMS-2 was drifted westward to 135°W longitude during the fall of 1975, and 10" x 10" photos are being read, the reduction of data will be extremely complex if its use becomes necessary. It is therefore presently planned to use only data from SMS-1 if possible. Figure 1 shows the areas of coverage of SMS-1 and -2.

The satellite imagery will be compared with solar radiation and sunshine data from the 18 stations shown in Figure 2. These were chosen because they had relatively long and reliable hourly records of simultaneous radiation and sunshine duration from the same locations. Most of the stations have information for each hour of the day for the five years 1952-1957. This is contained on magnetic tape compiled from records at the National Weather Records Center.

While many others have looked at the relationship between the two variables for one or two stations, (see [7] for a summary of such work) the broader coverage of this project requires that we establish such relationships for more stations representative of the various latitudinal and climatological regions of the U.S.A.

DATA ANALYSIS

A correlation analysis is being made on the five years of hourly sunshine and hourly solar radiation data for the 18 continental U.S. stations. The taped information has been grouped into monthly averages of each variable after classification by pairs of hours of the day, i.e., the two middle-hour values are considered as one, as are the earliest and latest, etc. using local solar time. These monthly values are then combined into seasonal values for the five years July 1952-June 1957 which are plotted for each station. In this way the data are still amenable to checking for accuracy, yet handled manually easily enough to reveal both the relationships between insolation and duration of sunshine for a given station as well as the differences which may exist between stations.

The aim of that portion of work is to determine whether one relatively simple relationship can be used for all continental U.S. locations for a given season. The complexity of the final computer analysis of the SMS-1 photographs will rise by nearly an order of magnitude if many areas are quite different from each other.

Figure 3 shows a typical gridded cloud photograph. The portion used to cover the U.S. is a small part of a 10" x 10" photograph which covers about one-fourth of the full disk image. The SMS-1 satellite spins at 100 revolutions per minute. The VISSR's scanning mirror faces the earth for about one-twentieth of each complete 360-degree rotation, scanning from west to east in eight identical visible channels and two redundant IR channels. The scan data is immediately transmitted in digital form to the Wallops Island, Va., Command and Data Acquisition station (CDA). While the spacecraft is completing its revolution, the mirror moves to the next southward step and scans again when it is looking at the earth once more.

Within 18.2 minutes the radiometer accomplishes the 1821 scan steps required to provide an image of the coverage area, Figure 1. The resulting visible images, made only in daylight, contain 14,568 lines and have a resolution of nearly 1/2-mile at the nadir point. IR images, acquired in darkness as well as in daylight, ////// have a total of 1821 lines, with 5-mile resolution. Allowing time for the scanning mirror to return to its starting point, and for correction of any "wobble" which may be caused by this retracting action, the Satellite Service scheduled GOES picture coverage at 30-minute intervals. That picture rate provided far more data each day than necessary for our studies.

At the CDA station, the eight lines of visible data acquired while the spacecraft looks earthward are gridded automatically and the rate of data transmission reduced, "stretched." As the satellite is completing its revolution and the VISSR is looking toward space, the stretched visible data signals are retransmitted from the CDA station through the satellite to the NESS at Federal Office Building number 4 in Suitland, Maryland and then relayed by microwave to the NESS Central Facility a few miles away.

Portions, such as those marked in Figure 3 of the analog grey scale 10" x 10" photographs received

from NOAA are being read on the television scanner of a GE Image-100 at NASA/KSC. This scanner produces 512 bits of information per line for 512 lines. The programmed output is a digital tape in ERTS format which will be processed on the University of Miami Univac 1106 computer. Three to five levels of cloud intensity will be used with an average space resolution on the order of 4-5 miles. The SMS VISSR imagery on our photographs has a basic resolution of one mile at the sub-point. This is degraded due to viewing angle about 18% at Miami to 1.18 miles and to about 3.77 miles at the far corner of the photograph near Seattle, Wash. Since the GE Image-100 will scan each photograph twice to cover the E-W U.S.A., but only once in the N-S direction, each of the 512 lines will correspond to about two of those on the photograph.

RELATIONS BETWEEN HOURS OF SUNSHINE AND SOLAR ENERGY

Figure 4 gives the annual mean daily solar radiation in Langleys (gram calories per square centimeter) based upon solar radiation measurements at a number of National Weather Service and cooperative observation stations in the United States [8]. The stations shown on this map do not represent the solar radiation data sources. Considering the fact that data from less than 85 stations in the 48 contiguous states were available, it is obvious that very much interpolation and extrapolation of the data was necessary to produce this map. Also, many of these stations have daily totalizers of radiation so that the hourly distribution of radiation cannot be determined from their past records. Relations exist between hourly radiation and hourly sunshine. Therefore, with good hourly sunshine and solar radiation data for only a few stations, the transform equations can be written to convert the vastly more detailed satellite data on hourly sunshine to equivalent Langleys of solar energy arriving at the earth's surface each hour.

Several factors enter into the relations between cloud free areas, or sunshine, as observed by the satellite and insolation received at the earth's surface. One important consideration is the time of day of maximum sunshine, whether morning and evening or midday. Two places with the same number of hours of sunshine per day can receive quite different amounts of solar energy depending upon this factor. Also, time of the year, station altitude, latitude, air pollution, and atmospheric moisture content are influential factors. Our derived relations between minutes of sunshine per hour and solar energy received are by hours of the day so that they can be used to convert the satellite measurments of sunshine to equivalent energy as a function of time of day. The 18 ground stations which we are using to develop these transform relations are widely dispersed so that they encompass different altitudes, latitudes, climates, and air quality. The relations derived for a particular station will be applied over the region around the station for which it is representative.

Many investigators have found good correlations between sushine and solar radiation received at a given place and time of year. However, most of them have compared daily total sunshine or percent of possible daily sunshine with the daily total radiation [7], [9], [10], [11], [12], [13]. Their results do not apply directly to our problem because they do not provide correlations between sunshine and radiation by hours of the day. They do provide a check on our results if we sum our hourly values of sunshine and radiation for all hours of the day.

Figures 5 and 6 are preliminary graphs of insolation versus minutes of sunshine per hour for pairs of morning and evening or midday hours at Madison, Wisconsin, for June and December. The hours are paired to give approximately equal sun angles fore and aft of noon true sun time (TST). These curves tend to show little seasonal change at the zero sunshine end of the scale because under such dense overcast conditions all of the energy received at the earth's surface is by the scatter mode. This is not affected greatly by the seasonal change in sun angle. Conversely, the clear sky or total sunshine end of the scale shows a much greater seasonal change because a large portion of the energy is direct and is sensitive to sun angle.

The sunshine switch used by the National Weather Service to measure minutes of sunshine per hour is biased. It is calibrated to register sunshine when a shadow is cast by nearby objects. This can occur with some degree of opaque clouds. At the other end of the scale, dense clouds must exist to register as zero sunshine. This means that a zero sunshine hour or day is truly cloudy, but a total sunshine hour or day may or may not be clear. Totally clear hours and days, particularly midday and in summer, should register slightly higher total insolation than is shown at the right in our curves.

Another graph similar to Figures 5 and 6 is being drawn for the combined spring and autumn relationship for Madison. The same seasonal graphs will be prepared for the other 17 stations shown in Figure 2. These will then be compared to determine how much, if any, the curves can be smoothed, and the geographical area over which each will be applied when converting cloudiness variables from the satellite photographs to insolation.

CONCLUSIONS

Ground measurements of solar radiation are too sparse to determine important mesoscale differences that can be of major significance in solar power station locations. A high positive correlation exists between recorded sunshine and solar energy received at a given place. Geostationary satellites can monitor sunshine (cloud free areas) throughout the day over large expanses of continents and oceans with great detail. Relationships can be derived between solar radiation and sunshine for different latitudes, seasons, and times of day by use of some existing records at a few stations. Computer techniques can apply these relationships to the satellite observations in order to obtain

detailed maps of land and water areas showing the best possible locations for solar power stations.

ACKNOWLEDGEMENTS

This research is supported by NASA, Goddard Space Flight Center contract NAS 5-22417. Dr. M. P. Thekaekara is the technical officer.

Both GSFC and the NOAA/National Environmental Satellite Service have provided some SMS-1 cloud images for processing. Personnel at Kennedy Space Center have assisted by reading some of these images onto computer tapes with their GE Image-100 and assisted in programming to print these on our Univac 1106 computer at the University of Miami.

Much valuable assistance in data analysis has been provided by graduate students S. T. Bukkapatnam and K. Akyuzlu. Eileen Kavlock assisted in preparing this manuscript.

REFERENCES

[1] NOAA, Environmental Research Laboratories, Report of Solar Energy Data Workshop, 29-30 November 1974, NSF-RA-N-74-062, Air Resource Laboratories, Silver Spring, Maryland, 218 pp.

[2] Hiser, H.W. and H.V. Senn, "Determining Potential Solar Power Sites in Western Hemisphere Ocean and Land Areas Based Upon Satellite Observations of Cloud Cover," Remote Sensing: Energy-Related Studies, edited by T. Nejat Veziroglu, Halsted Press, New York, 1975, pp. 247-260.

[3] Fritz, S., P. Krishna Rao and M. Weinstein, "Satellite Measurements of Reflected Solar Energy and the Energy Received at the Ground," Jour. of the Atmos. Sciences, Vol. 21, March 1964, pp. 141-151.

[4] Thekaekara, M.P., et al., "Solar Irradiance Measurements from a Research Aircraft," Applied Optics, Vol. 8, No. 8, 1969, pp. 1713-1732.

[5] Hanson, K.J., "Studies of Cloud and Satellite Parameterization of Solar Irradiance at the Earth's Surface," Proceedings of the Miami Workshop on Remote Sensing, Environmental Research Labs., NOAA, Boulder, Colorado, July 1971, pp. 133-148.

[6] Vonder Haar, T.H. and J.S. Ellis, "Solar Energy Microclimate as Determined from Satellite Observations," presented at the 19th Annual Tech. Symposium, Optics in Solar Energy Utilization, Society of Photo-Optical Instrumentation Engineers, San Diego, California, 1975.

[7] Viswanadham, Y. and R. Ramanadham, "The Relation Between Solar Radiation and Hours of Bright Sunshine at Some Tropical Stations," Pure and Applied Geophysics, Vol. 74, 1969, pp. 186-194.

[8] Environmental Data Service, Climates of the United States, NOAA, 1973.

[9] Lund, I.A., "Relationships Between Insolation and Other Surface Weather Observations at Blue Hill, Massachusetts," Solar Energy, 1968, pp. 95-106.

[10] Hamon, R.W., L.L. Weiss, and W.T. Wilson, "Insolation as an Empirical Function of Daily Sunshine Duration," Monthly Weather Review, Vol. 82, No. 6, June 1954, pp. 141-146.

[11] Black, J.N., C.W. Boynthon, and J.A. Prescott, "Solar Radiation and the Duration of Sunshine," Royal Met. Soc. Quarterly Jour., Vol. 80, 1954, pp. 231-235.

[12] Glover, J. and J.S.G. McCulloch, "The Empirical Relation Between Solar Radiation and Hours of Sunshine," Royal Met. Soc. Quarterly Jour., Vol. 84, No. 360, 1958, pp. 172-175.

[13] Waite, P.J. and R.H. Shaw, "Solar Radiation and Sunshine in Iowa," Iowa State Jour. of Science, Vol. 35, No. 3, 1961, pp. 355-365.

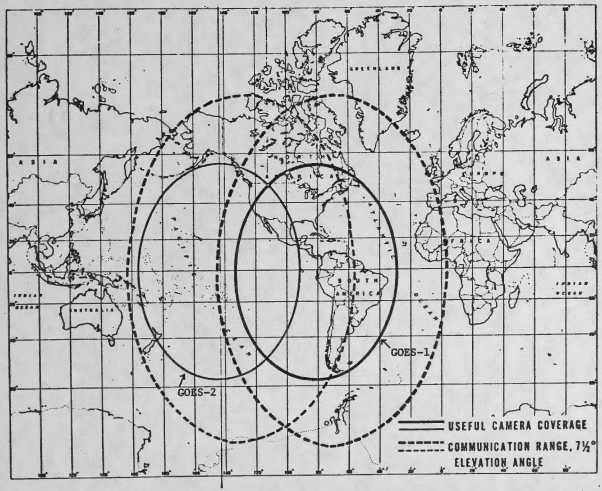

Figure 1. Typical coverage from a 2-GOES system showing area of useful camera coverage and communications range at 7.5-degree antenna elevation for data collection and relay.

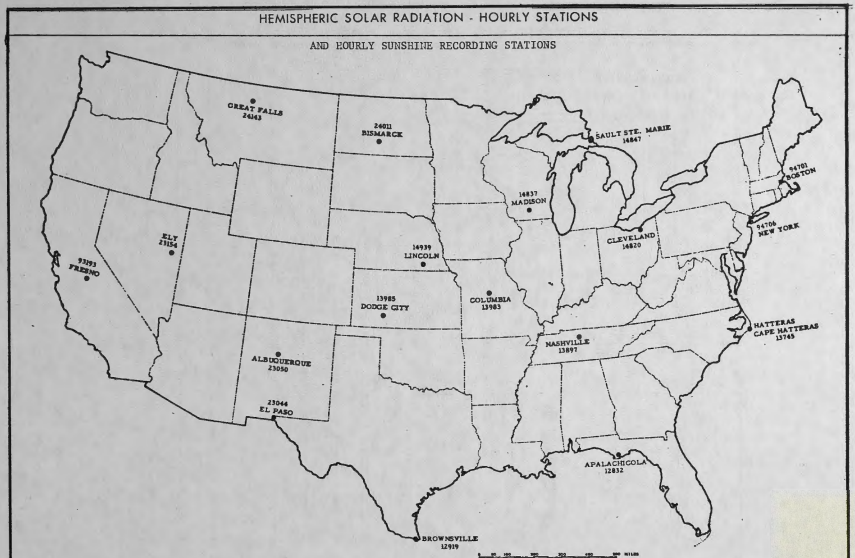
HEMISPHERIC SOLAR RADIATION - HOURLY STATIONS
AND HOURLY SUNSHINE RECORDING STATIONS
GREAT FALLS
24143
24011
BISMARCK
SAULT STE. MARIE
14847
94701
BOSTON
14837
MADISON
94706
NEW YORK
CLEVELAND
14820
ELY
23154
93193
FRESNO
14939
LINCOLN
13985
DODGE CITY
COLUMBIA
13883
HATTERAS
CAPE HATTERAS
13749
NASHVILLE
13897
ALBUQUERQUE
23050
23044
EL PASO
APALACHICOLA
12832
BROWNSVILLE
12919

Figure 2

Figure 3. Visible Spectrum Image of Clouds Over the United States from SMS-1, Geostationary Satellite, 1800 GMT, 1 January 1975.